Renewable Energy 86 (2016) 831–840

Contents lists available at ScienceDirect

Renewable Energy

journal homepage: www.elsevier.com/locate/renene

Evaluation of WRF shortwave radiation parameterizations in predicting Global Horizontal Irradiance in Greece

Melina-Maria Zempila [a, *], Theodore M. Giannaros [b], Alkiviadis Bais [a], Dimitris Melas [a], Andreas Kazantzidis [c]

[a] Laboratory of Atmospheric Physics, Aristotle University of Thessaloniki, PO Box 149, 54124, Thessaloniki, Greece
[b] National Observatory of Athens, Institute for Environmental Research and Sustainable Development, Vas. Pavlou & Metaxa, 15236, Athens, Greece
[c] Laboratory of Atmospheric Physics, University of Patras, Physics Department (Building B), 26500, Rio, Greece

ARTICLE INFO

Article history:
Received 28 April 2015
Received in revised form
2 July 2015
Accepted 25 August 2015
Available online 18 September 2015

Keywords:
Global Horizontal Irradiance
Numerical modeling
WRF
Shortwave radiation parameterizations
Hellenic Network of Solar Energy
Aerosol effects

ABSTRACT

This study aims at assessing the differences induced in the Global Horizontal Irradiance (GHI) predictions by the mesoscale atmospheric Weather Research and Forecasting (WRF) model when using different shortwave radiation. Model predictions are compared with GHI measurements at 12 stations of the Hellenic Network of Solar Energy (HNSE) for January, April, July and October 2013. The shortwave radiation schemes that were evaluated are: the Dudhia, the updated Rapid Radiative Transfer Model (RRTMG), the updated Goddard and the Goddard Fluid Dynamics Laboratory (GFDL) schemes. All schemes perform better under cloudless conditions due to limited ability of the WRF model to simulate cloudy conditions. The Dudhia scheme performs best with mean relative difference of 2.2 ± 15% for clear-skies, while the differences for the other schemes range between 5 and 12% with similar standard deviations. For all-skies, the model-derived hourly GHI is overestimated for all schemes (~40–70%).

For the daily averages, the model predictions are in better agreement with the measurements, mainly under all-sky conditions, with deviations of about half those of the hourly data and smaller standard deviations. There are strong indications that the differences of the model predictions from the measurements depend on the solar zenith angle and the amount of aerosols at each station.

1. Introduction

Renewable energy resources have been attracting significant interest throughout the past decades due to rapid depletion of conventional fossil fuels and the environmental problems arising from their extensive use in the past. Solar energy, in particular, is considered to be a very attractive solution for power generation since it is undoubtedly the most abundant renewable resource [53,7,49]. According to the 2012 report of the International Energy Association (IEA), solar electricity production exhibited a mean growth rate of 23.4% from 1990 through 2011 [26]. In particular during the past few years, the solar energy market has significantly expanded, reaching a maximum 74.1% growth rate in 2011 [26], while the share of renewables in power generation increases most in OECD countries (37%). Globally, solar technologies share a growth of 18% in renewables-based generation ([27]; Executive Summary). Whilst the wind and solar PhotoVoltaic (PV) exploitation in the world's power demand quadruples, their integration to the existing electricity infrastructure becomes more challenging, with solar PV accounting for 37% of summer peak demand in Japan [27]; Executive Summary).

Solar electricity production can be either based on direct normal irradiance (DNI), exploitable in solar thermal power plants (e.g. Refs. [15,17,39,51]), or Global Horizontal Irradiance (GHI), applicable to photovoltaic systems (e.g. Ref. [33,34,38,41,44,47,48,55]). In both cases, weather conditions play an important role by shaping the highly fluctuating character of solar radiation. This poses major challenges for the integration of solar power production systems into existing energy supply infrastructures. Past experience (e.g. Refs. [3,28]) has shown that although accurate predictions of a renewable power such as solar is a demanding task, however a geographical distribution of the solar PV plants can lead to a smoother aggregated power production [60,10,35,32,56], while supplementary improvement solutions were discussed by Kiliccote et al. [30] and Hart et al. [21].

Numerical Weather Prediction (NWP) models are considered a

* Corresponding author.
E-mail address: mzempila@auth.gr (M.-M. Zempila).

http://dx.doi.org/10.1016/j.renene.2015.08.057
0960-1481/

valuable tool for the assessment and forecasting of solar power availability [42]. In particular, the capability of such models in terms of predicting GHI accurately has been attracting increasing attention in recent years. As early as in the beginning of 2000's, Zamora et al. [61,62]; examined the ability of the mesoscale Fifth-Generation Penn State/NCAR Mesoscale (MM5) model [18] for simulating GHI in the US Heinemann et al. [22]. also employed MM5 for evaluating two-day-ahead forecasts of GHI in Germany. More recently Lara-Fanego et al. [31]; conducted a comprehensive evaluation of the Weather Research and Forecasting (WRF) model [50] solar irradiance predictions in the area of Andalusia, Spain, while Ruiz-Arias et al. [45] evaluated different shortwave radiation schemes in WRF by comparing predictions with measurements of the SURFRAD network in the US. An overview of studies employing NWP models for solar irradiance forecasting is available in Perez et al. [42].

In accordance with the Directive 2009/28/CE of the European Union, the goal for Greece was to achieve a 20% share of renewable energy resources in the total energy production by 2020 [23]. In this context, the number of studies focusing on the country's solar energy production has been recently growing (e.g. Refs. [12,13,59]). However, to the authors' knowledge, there are currently no detailed studies for the evaluation of the predictions of solar irradiance in Greece with NWP models. Taking into account the previous discussion, the latter is essential for facilitating the integration of solar power production into the electrical grid and for achieving the target of 20% share in energy production.

The aim of the current study is the evaluation of the WRF model that is used regularly for providing forecasts of GHI over Greece by comparison to measurements at different stations of the Hellenic Network of Solar Energy (HNSE) network. Although it was suggested [43] that WRF should not be regarded as a state-of-the-art model for GHI predictions it is still widely used in such applications.

The study focusses mainly on the investigation of the model's sensitivity to the parameterization of shortwave (SW) irradiance. To this end, numerical experiments were conducted for four monthly periods in year 2013. The impact of geographical and seasonal variations as well as of sky conditions on the performance of the model is examined and discussed. In addition, a simple approach is followed for investigating the impact of variations in aerosol optical depth on the model-derived GHI.

2. Methodology

2.1. Study area and observations

Greece is situated at the southeastern end of the European continent (Fig. 1a), between 34° and 42° northern latitude, and 19° and 28° eastern longitude, comprising a mountainous peninsular mainland in the southeast Mediterranean region, and covers an area of approximately 132,000 km^2.

Greece is characterized by abundant solar potential due to its geographical position and climatological regime. According to Matzarakis and Katsoulis [36]; in the interior mountainous areas (Western Macedonia, Epirus, Central Greece) the annual and seasonal bright sunshine is lowest and increases towards the coasts of the Ionian and Aegean seas, and towards the southern part of Greece. As it appears from the sunshine duration records of the Hellenic National Meteorological Service, for the years 1960–1990 the lowest values of annual sunshine duration were found in Mikra (40.31° N, 22.58° E), while Ierapetra (35° N, 25.35° E) experienced the highest values reaching more than 3000 h of sunshine annually. Therefore, Greece has a strong potential of solar electricity generation, especially during cloudless summer days. For example, a typical crystalline silicon PV system established in an urban residential area in Greece can produce annually between 1100 and 1330 kWh per installed kW$_p$ [52].

The measurements used in this study were obtained from a network of 12 stations equipped with Kipp & Zonen pyranometers (types CM10, CM11 and CM21). The aforementioned pyranometers comply with the specifications of the first class “High Quality” as defined in the “Guide to Meteorological Instruments and Methods of observation”, of the World Meteorological Organisation (WMO). The installation of instruments started in 2011 in the frame of the Hellenic Solar Network (HSNE) project [2] and was completed in 2012. The locations of the stations, shown in Fig. 1b and summarized in Table 1, were selected to represent, as much as possible, regions with different cloud coverage characteristics [20,58,59] to account for the variability in solar irradiance due to regional weather and cloud regimes. At all stations the field of view of the pyranometers is unobscured by local obstacles, at least for solar zenith angle (SZA) smaller than about 80°. Before deployment in the network stations, all instruments were first calibrated in the laboratory by comparison to a standard instrument using a 150 W Halogen radiation source. The measurements derived from the network of pyranometers include one-minute data of GHI together with the respective standard deviation of the values recorded within each minute (usually between 50 and 60).

2.2. Model setup

The meteorological model used in the present study is WRF, version 3.5.1 [50]. Two one-way nested modeling domains were specified (Fig. 1a) with horizontal grid spacing of 30 km (DO1, mesh size of 133 × 75) and 10 km (DO2, mesh size of 112 × 100), of which the innermost domain focuses on the study area. In the vertical, thirty unevenly spaced full sigma levels were defined for both domains, with the model top set at 100 hPa. Microphysics were handled with the Thompson scheme [54], while the Grell–Devenyi [19] ensemble scheme was chosen for parameterizing convection. The Mellor–Yamada–Janjic scheme [29] was used for representing boundary-layer processes and Noah [8] was selected as a land-surface model. Longwave radiation processes were parameterized with the updated Rapid Radiative Transfer (RRTMG) scheme [25].

2.2.1. Sensitivity experiments

Several numerical experiments were conducted to investigate the sensitivity of GHI predictions to the selection of a particular SW radiation scheme. In this context, the examined SW radiation parameterizations include (a) the Dudhia scheme [11], (b) the updated Rapid Radiative Transfer Model (RRTMG) scheme [25], (c) the updated Goddard scheme [9], and (d) the Goddard Fluid Dynamics Laboratory (GFDL) scheme [14]. Default total ozone and no explicit aerosol data were considered in the numerical simulations conducted with each of the above SW radiation schemes. However, for Dudhia scheme extinction by aerosols is implicitly included in the empirical scattering scheme representing average turbidity conditions [61,62].

Due to restrictions in computational capacity, four months in the year 2013, (i.e. January, April, July, October) representing the four seasons, were specified for carrying out the numerical experiments. Within each month, WRF simulations were initialized at 12:00 UT every four days using 1° × 1° spatial and 6 h temporal resolutions. Operational surface and upper-air atmospheric reanalyses data were provided by the National Centre for Environmental Predictions (NCEP). The duration of the simulations was set to 84 h with the model providing output data at 1 h intervals. The first 12 h of each simulation were discarded as coinciding with the model's spin-up period and evaluation was conducted using the remaining 72 h of model data.

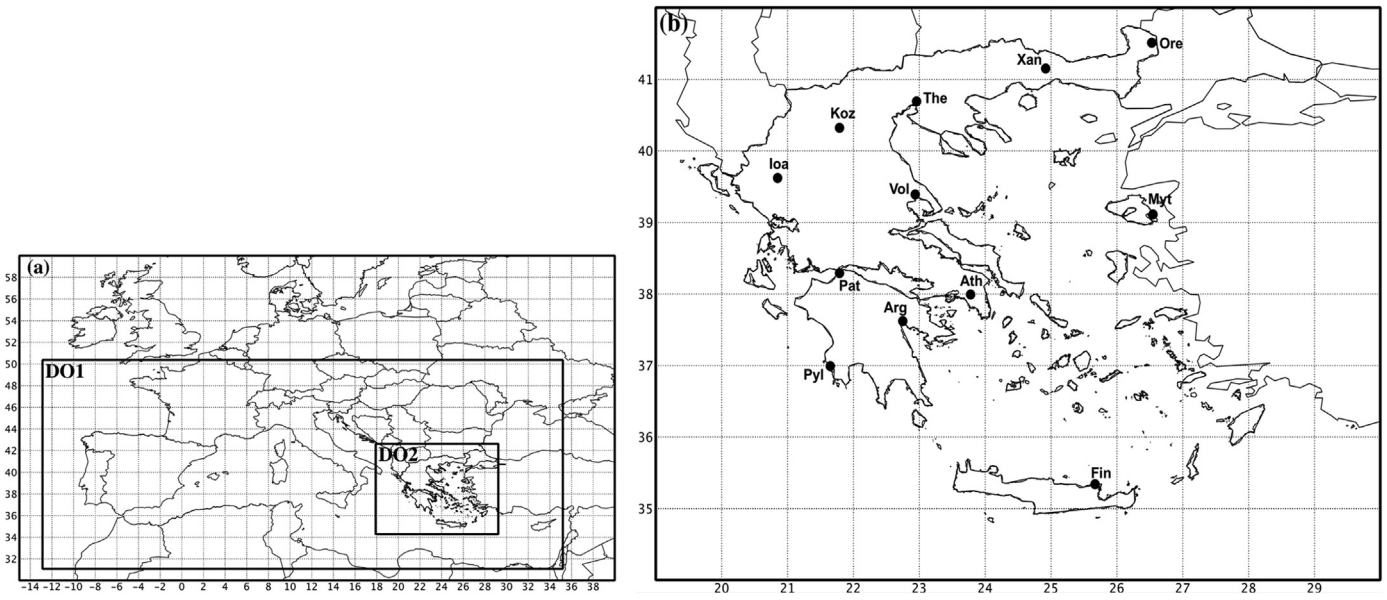

Fig. 1. Modeling domains (a) and locations of the Hellenic Network of Solar Energy (HNSE) stations used in the study (b).

Table 1
Location and type of pyranometer used for GHI measurements at the monitoring stations of HSNE.

Station	Station abbreviation	Latitude (°N)	Longitude (°E)	Altitude (m)	Pyranometer type
Athens	Ath	37.99	23.78	180	CM21
Argos	Arg	37.62	22.75	22	CM11
Finokalia	Fin	35.34	25.67	250	CM11
Ioannina	Ioa	39.62	20.85	541	CM10
Kozani	Koz	40.32	21.79	719	CM10
Mytilene	Myt	39.11	26.55	80	CM11
Orestiada	Ore	41.51	26.53	44	CM10
Patra	Pat	38.29	21.79	70	CM11
Pylos	Pyl	36.99	21.65	22	CM21
Thessaloniki	The	40.69	22.96	60	CM21
Volos	Vol	39.39	22.94	50	CM21
Xanthi	Xan	41.14	24.89	75	CM11

At this point it is worth noticing that for the evaluation of the model's performance, no discrimination of data was applied based on the simulation lead-time. This decision can be justified by the fact that all numerical simulations were driven by re-analyses data and thus, the impact of time horizon on model performance is expected to be low. More importantly however, such an analysis was performed and revealed a negligible impact of simulation lead-time on model performance.

2.3. Evaluation procedure

The performance of WRF in terms of simulating GHI was evaluated using in situ data from the 12 stations of the HSNE network (Table 1). The model-predicted GHI data were first interpolated onto the locations of the measurement sites, using a simple nearest-neighbor approach. The interpolated model data were then compared to concurrent quality assured GHI observations.

In order to match model results to observations, the interval at which WRF calls the SW parameterization was taken into account. In the conducted numerical experiments this interval was set to 30 min. Consequently, SW irradiance was computed at the middle of this interval, so that the corresponding value is representative of the whole period between two successive calls to the parameterization. Hence, WRF SW irradiance was computed at min 15 and 45 of each hour. Considering this, it would be ideal to compare the GHI measurement 15 min before each hour with the corresponding hourly model output. However, to compensate for the spatial differences between the model and the measurements the average GHI a few minutes before and after this minute would have been more representative. An averaging interval of ±5 min would have been more appropriate in order to avoid influences from the changing SZA during this interval, particularly for clear skies. On the other hand though, a larger interval would account better for the effects of changes in cloudiness within each grid which cannot be resolved by the model. Therefore averages of GHI within ±15 min were used in the comparisons, although the short interval gives slightly better results for clear skies. A similar matching approach was followed in the recent work of Ruiz-Arias et al. [45]. While averages of GHI from the measurements derived from at least 15 min measurements were included in the comparisons.

The statistical quantities computed to quantitatively assess the performance of WRF under the different numerical experiments include: (a) the mean of the percentage differences relative to the observed GHI (RD): 100 × (Model-Observation)/Observation, (b) the standard deviation of RD for the data of all the 12 Hellenic Network of Solar Energy (HNSE) stations (STD, Eq. (1)), and (c) the root mean squared error (RMSE, Eq. (2)). In Eqs. (1) and (2), n denotes the number of observation–prediction pairs used in the

evaluation, while o_i and m_i stand for the observed and modeled GHI data, respectively.

$$STD = \sqrt{\frac{1}{n-1}\sum_{i=1}^{n}((m_i - o_i)/o_i - \frac{1}{n}\sum_{i=1}^{n}((m_i - o_i)/o_i)^2} \quad (1)$$

$$RMSE = \sqrt{\frac{1}{n}\sum_{i=1}^{n}(o_i - m_i)} \quad (2)$$

The evaluation of the WRF experiments was carried separately for clear-sky and all-sky conditions, identified from observations combined with simulations with the uvspec [37] radiative transfer model (RTM).

In particular, every individual minute is characterized as cloud-free or not by combining and comparing GHI measurements with estimations for clear skies resulting from the uvspec model. In the model runs we assumed a high aerosol optical depth (AOD), 0.4 at 500 nm, and an Angstrom exponent of 1.3, representing the smallest possible GHI under clear skies for each particular location [16,40]. Only GHI data higher than the corresponding model estimate are considered as clear sky measurements, assuming that values smaller than this limit are influenced by clouds. In addition, 1-min measurements with standard deviation larger than 10% of the mean were also considered as influenced by clouds and removed from the clear-sky dataset. Finally, the percentage errors of the normalized to the data point of interest model estimations on five adjacent observations, centered at each data point, were computed. For SZAs smaller than 75° a data point is characterized as cloud-free when the differences agree to within 2%. For larger SZAs agreement to within 5% is required. From the minute observations of GHI the "clear-sky" means for 30 min intervals are calculated as long as more than 20 data points are characterized as "clear-sky". The evaluation of the algorithm for Thessaloniki revealed an agreement of better than 80% compared with observations of cloudiness.

3. Results and discussion

3.1. Sensitivity to solar zenith angle

Before evaluating the overall model performance, the diurnal behavior of the GHI predictions for each scheme was investigated for cloud-free cases, as determined both from the measurements and the model. In this case the ±5 min averages of GHI measurements were used to improve the comparisons at large SZAs. As seen in Fig. 2, for Thessaloniki, there is a diurnal dependence of the ratio model to measurements in three of the SW radiation schemes. The magnitude of this dependence varies among models, and because it is symmetric with respect to local noon it can be associated with the variation of SZA. Generally, all models overestimate the GHI throughout the day. Dudhia's scheme shows the smallest SZA dependence, of the order of 5–10%, while the GFDL scheme shows the largest diurnal pattern with overestimation up to 50% at SZAs around 80°. The other two schemes show similar behavior with largest overestimation of 20–25%. Apparently, there is also a seasonal dependence of the model-to-measurements ratio, with April and July showing smaller and less SZA-dependent deviations compared to October and January. These seasonal differences could be due to aerosols which are more abundant during the warm period, leading to reductions in the measured GHI, while the model estimates are unaffected. The large diurnal variations cannot be attributed to measurement errors since the angular response error of this type of pyranometers is substantially lower (nominally ±2% at SZA 60° and ±6% at SZA 80°). It should be noted that this error applies mainly to the direct irradiance component; therefore for large SZAs the angular response error in GHI would be even smaller. The large deviations of the ratios at large SZAs may have been caused by obstacles close to the horizon, other local effects, and by uncertainties in the measured GHI which at these SZAs has very small values. Finally, the noise in the ratio can be attributed to effects from varying aerosols, thin clouds that were not captured by the cloud screening algorithm, variations in water vapor which are not taken into account, and by uncertainties in the model estimates.

The patterns shown in Fig. 2 are typical for all stations as far as it concerns the general shape, although there are differences with respect to absolute deviations. This is an additional indication for the effects of aerosols which differ in quantity among stations, and will be discussed later in more detail.

Since the diurnal patterns occur at all stations, it is reasonable to assume that they are not caused by the measurements, but likely by the radiation schemes. Therefore, the comparisons of the hourly data and the relevant statistical analyses are restricted to data corresponding to SZA of less than 70°, as a compromise between the model errors and the actual GHI levels.

3.2. GHI predictions: hourly means

Table 2 summarizes the RD and RMSE, averaged over all stations and monthly periods, as a function of sky conditions. The number of data pairs used was 9420 for all-sky and 3869 for clear-sky conditions. Not surprisingly, all schemes are found to perform better for clear-skies. This can be attributed to the generally limited ability of the model to simulate accurately short-term (e.g., hourly) variations in irradiance under cloudy conditions (e.g. Refs. [31]); especially since the properties of clouds and their exact position cannot be accurately predicted by NWP models, as well as to the fact that the model estimates represent average conditions over a specific grid, while the measurements are representative of a single location.

The Dudhia scheme, which is the simplest, performs best irrespectively of sky conditions. For clear skies, all models except the GFDL are in good agreement with the measurements, with average differences of 2–8%. The relative standard deviation (RSD) for all schemes is about 14% denoting that the results are consistent in terms of variability. These values are relatively large and may arise from differences in the atmospheric conditions among stations, as well as from the fact that the means are formed by all hourly ratios including those at large SZAs which bias the averages towards higher values and increase the standard deviations.

For all skies, the Dudhia scheme results in an average overestimation of the model of about 40%, while for the other three schemes the overestimation is even larger, by 20–30% more. One would expect a larger variability in the model forecasts under all-sky conditions, because of the large variability in cloudiness, but not a systematic overestimation. This means that all models mostly predict less cloud attenuation than actual leading to large positive RD.

The relative standard deviations are very large under all skies, ranging between about 230 and 340%, suggesting very large variability of the hourly relative differences. This is because cloud effects are extremely difficult to be predicted accurately within 30-min intervals, while the spatial inhomogeneity of clouds introduces additional uncertainties when comparing single point measurements with gridded model simulations. The large standard deviations might also be connected to the different regimes of cloudiness amongst the 12 stations, and might imply that at some stations the model-to-measurement differences are much larger.

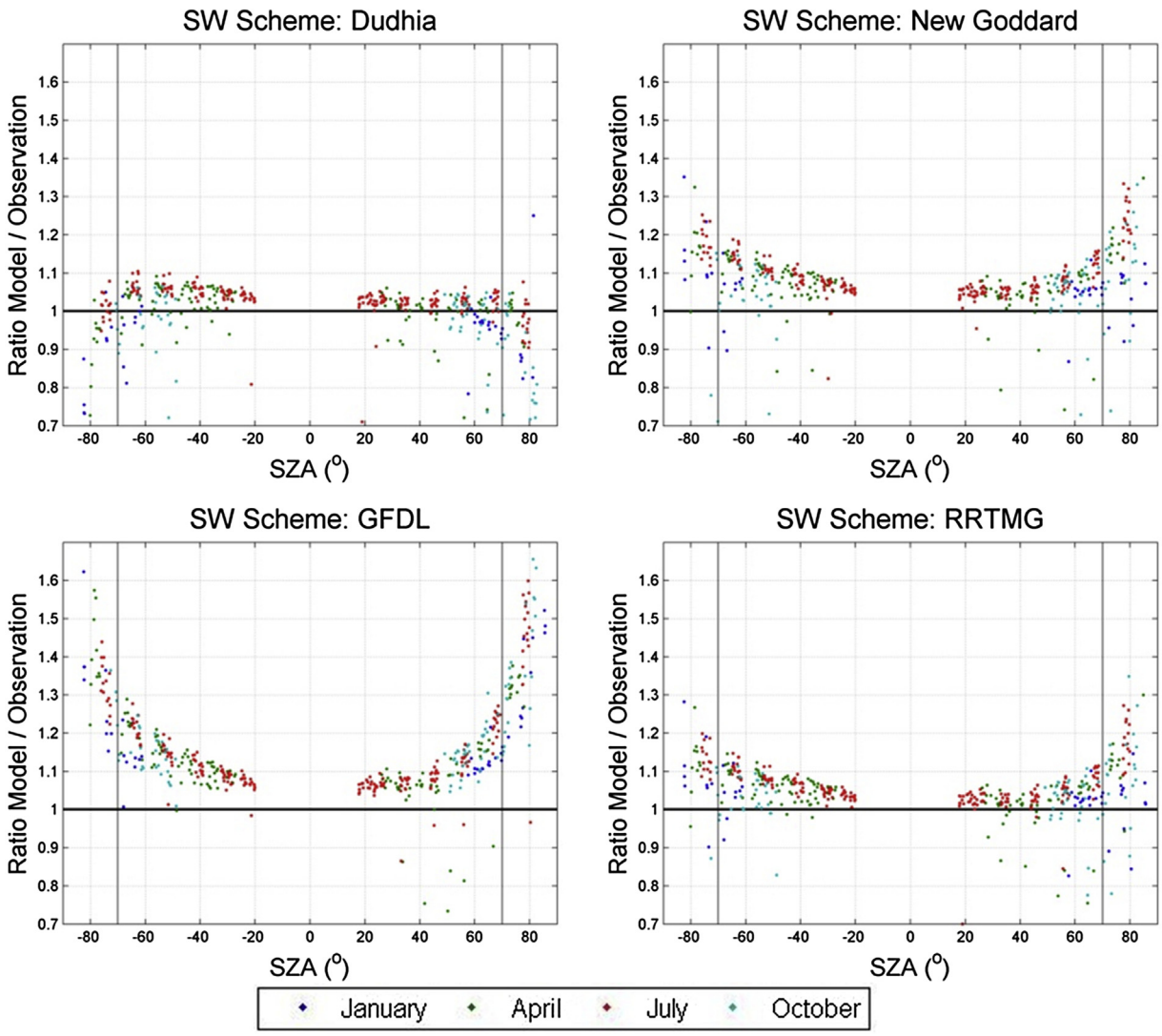

Fig. 2. Solar zenith angle dependence of the ratio model/measurements under clear skies for Thessaloniki. Each panel corresponds to a different SW radiation scheme. Data points for different months are plotted in different colors. Negative SZAs correspond to morning hours (i.e. before local noon) (For interpretation of the references to color in this figure legend, the reader is referred to the web version of this article.).

Table 2
Mean relative differences (RD) with standard deviation (in parentheses) expressed in percent and root mean squared error (RMSE) of hourly GHI for all stations and monthly periods, for clear-sky and all-sky conditions.

	Clear skies		All skies	
	RD (%)	RMSE (W m^{-2})	RD (%)	RMSE (W m^{-2})
Dudhia	2.25 (15.58)	102.03	42.63 (228)	185.45
New Goddard	7.73 (14.16)	103.74	56.49 (276)	195.02
GFDL	12.24 (13.63)	112.89	73.12 (337)	212.38
RRTMG	5.28 (13.13)	92.75	56.40 (269)	187.28

This is investigated by examining the average deviations for individual stations using the hourly data for the whole year (Fig. 3). For example, the GHI under clear skies in Pylos is strongly overestimated in all SW schemes, while in Patras the deviations are much smaller. For the Dudhia scheme average differences close to zero or even small underestimation of the predicted GHI are encountered in several stations. The deviations for the other three schemes are larger, about 5% for New Goddard and RRTMG and more than 10% for GFDL. Differences in the standard deviations amongst stations are most likely due to different cloud regimes, while differences in absolute level could arise from various factors: first, due to the actual aerosol optical properties which are not taken into account in the model, and second, due to differences between the actual amount of water vapor relative to that predicted by the model. Aerosols may cause a reduction in the measured GHI, while difference in the water vapor can lead either to reductions or to increases in GHI. Finally, the topography within each grid and around each station may also play a role, as well as the particular characteristics of each SW radiation scheme. For the station data (Obs), topography can cause also seasonal effects at relatively large SZAs, because surrounding mountains may block the direct solar radiation differently in different seasons due to seasonal changes in the solar azimuth. Such effects are not accounted in the radiation schemes.

As discussed already, model deviations for all skies are larger (ranging between 20 and 100%). The systematic large overestimation seen in the averages of Table 2, are also shown for individual stations, confirming that this is likely a model feature and does not arise from the measurements. The RSDs at some stations reach 600–800% and are revealed to be systematic for all schemes.

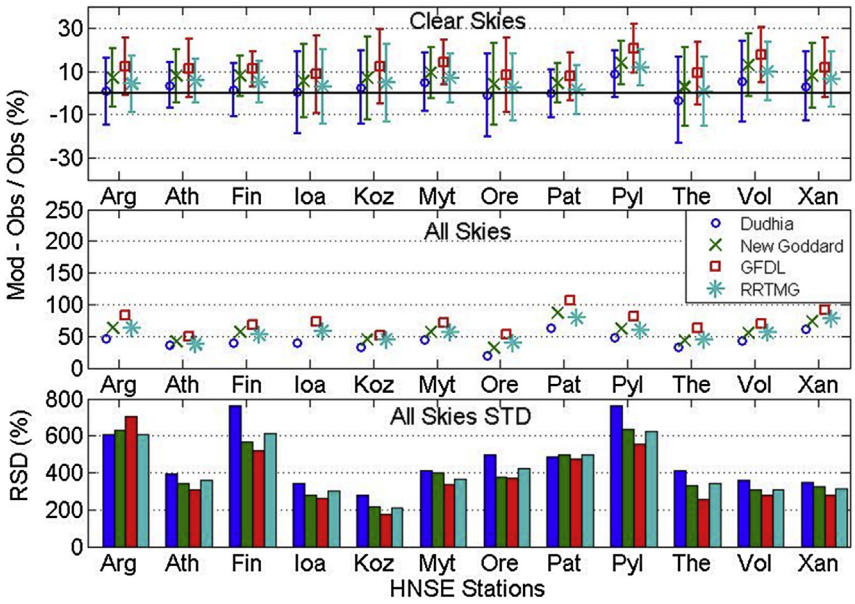

Fig. 3. Mean differences in (%) of model derived hourly GHI relative to measurements at each station of HNSE for the whole period of study, separately for clear skies (upper panel) and all skies (middle panel). Different symbols are used for each SW radiation scheme. Vertical bars in the upper panel correspond to one standard deviation of the data entering the mean. For all skies, the standard deviation is very large and is shown separately as a bar chart (lower panel).

This suggests that the main cause is local cloud regimes that are not captured by the hourly model predictions (Mod) of clouds.

To assess the importance of seasonal effects in the comparison results, monthly-mean relative differences were calculated for each of the four months using all available data, which are shown in Table 3.

For clear skies, differences among months are relatively small; the order of 3–5% for all schemes, and the variability is quite large. The Dudhia scheme exhibits the largest overestimation (3.7%) in July, while in January the predictions are underestimated by about 6%. In accordance with the annual statistics (Table 2), the other schemes overestimate the GHI by 2–17%. The results are much different for all-sky conditions. The absolute differences increase substantially by up to 4 times in January and October relative to July, while in April differences are about double those of July. As for the relative standard deviations these are still large, comparable to those seen in the annual statistics (see Table 2).

To conclude with the assessment of the hourly predictions, it appears that for clear skies the agreement between the predictions and the measured data are within acceptable ranges, at least for the scheme of Dudhia, and possibly for RRTMG and New Goddard. However for all skies, both in absolute level and in terms of variability the four schemes fail to predict within acceptable limits the measured GHI on hourly basis. Since the comparisons are for 30-min intervals every hour both for the measurements and the model, it is reasonable to expect large discrepancies from model calculations over a 10 × 10 km grid.

3.3. GHI predictions: daily averages

The Daily averages of GHI, based on common hourly data points, were also calculated and compared for days with data availability of more than 50%, and with at least 2 data points around local noon (i.e. for 9:45 and 10:45 UT). Because of these limitations, the clear-sky dataset from all stations comprises 983 days.

For clear skies and for all schemes, the relative deviations for the daily data have not changed substantially compared to hourly. However, the standard deviations have been reduced to about half, due to the suppression of the GHI variations within the day (Table 4). The average overestimation is smaller by about 0.8–1.4% than for the hourly data. For all skies, the relative deviations for daily data are about half those for the hourly, ranging between 25 and 45%. Similarly, the variability of the differences is considerably smaller, with the standard deviations ranging between 79 and 94%; at least 3 times smaller than for the hourly data. Once again, the Dudhia scheme agrees better with the measurements both for clear-sky and all-sky conditions.

When examining the stations individually the average deviations of the model estimates from the measurements for clear skies range between −5% and 20% for all stations and schemes (Fig. 4). For the Dudhia scheme, the deviations are even smaller; the smallest (within ±2% are found in Argos, Mytilene, Patras and Thessaloniki, and the largest (up to ~10%) for Xanthi and Pylos). For all skies, most stations show deviations ranging between about 20% and 50%, except for Orestiada where deviations range from 10 to

Table 3
Monthly mean relative differences (in %) of model derived hourly GHI relative to measurements from all stations, separately for clear-sky and all-sky conditions, for each SW radiation scheme. Values in parentheses denote the standard deviation.

	Clear skies				All skies			
	Jan.	Apr.	Jul.	Oct.	Jan.	Apr.	Jul.	Oct.[a]
Dudhia	−5.9 (22.1)	1.78 (14.4)	3.69 (15.8)	0.66 (12.6)	65.48 (254)	44.62 (161)	21.79 (106)	72.51 (443)
New Goddard	4.94 (16.6)	7.35 (13.1)	8.12 (15.2)	7.75 (11.1)	92.87 (313)	59.56 (226)	27.21 (104)	91.82 (521)
GFDL	13.26 (13.7)	10.77 (14.2)	11.72 (14.2)	16.57 (8.8)	124.78 (408)	69.17 (205)	33.78 (114)	131.78 (676)
RRTMG	1.91 (17.8)	5.49 (11.5)	5.56 (14.0)	4.98 (10.1)	96.49 (309)	59.45 (224)	25.21 (106)	93.21 (496)

[a] Data from 7 out of 12 HNSE stations were included in October's mean (Argos, Finokalia, Ioannina, Orestiada, Patras, Pylos and Thessaloniki).

Table 4
Mean relative differences (RD) with standard deviation (in parentheses) expressed in percent and RMSE of daily GHI for all stations and monthly periods, for clear-sky and all-sky conditions.

	Clear-skies		All-skies	
	RD (%)	RMSE (kWh m^{-2})	RD (%)	RMSE (kWh m^{-2})
Dudhia	2.21 (7.21)	0.356	23.96 (79.48)	1.025
New Goddard	6.89 (6.88)	0.487	32.69 (78.89)	1.155
GFDL	10.81 (7.21)	0.610	43.97 (93.80)	1.341
RRTMG	4.41 (6.47)	0.386	32.42 (84.37)	1.099

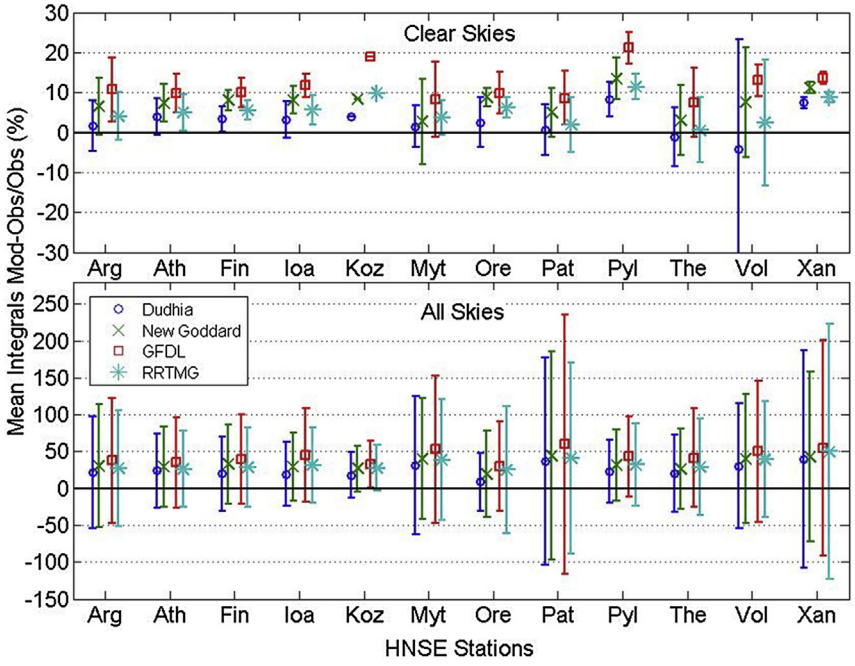

Fig. 4. Mean differences in (%) of model derived daily GHI relative to measurements at each station of HNSE for the whole period of study, separately for clear skies (upper panel) and all skies (lower panel). Different symbols are used for each SW radiation scheme. Vertical bars correspond to one standard deviation of the data entering the mean.

30%. The relative standard deviations are now much smaller than in the hourly data, therefore, allowing plotting error bars in the respective panel of Fig. 4. Differences between stations do not reveal any particular geographical pattern and most likely result from individual characteristics of the stations' topography and instruments' field of view and stability.

3.4. Sensitivity of SW radiation schemes to aerosol optical depth

None of the numerical experiments accounted explicitly for the effects of aerosols on SW irradiance, therefore it would be expected that the GHI estimations would be positively biased. This effect should reveal some seasonal characteristics, due to the distinct seasonal variability of aerosols at all stations. To identify and possibly quantify these effects, the ratio of modeled to measured GHI is examined as function of aerosol optical depth (AOD) measurements at 675 nm derived by CIMEL sun-photometers operating at four AERONET (AErosol RObotic NETwork, NASA) stations which are in close proximity with the corresponding HNSE stations. Level 1.5 data were used instead of the higher quality level 2.0, to increase the number of data pairs entering the comparisons. When available, the closest (within 30 min) AOD mean values were matched with the hourly clear-sky model-to-measurement GHI ratios. Due to scarcity of the Cimel data and the gaps in the HNSE stations, the availability of common data is rather poor, particularly during the winter, as it appears from Table 5. The best data coverage is for Thessaloniki in July and October and for Athens in April and July. The available data pairs are marginally sufficient for Finokalia, and insufficient for Xanthi to derive meaningful statistics.

Fig. 5 shows the model-to-measurement ratios as a function of AOD at 675 nm (AOD @ 675 nm) for the four SW schemes and for each of the four stations. Despite the significant scattering of the data, which is greatest for GFDL, a tendency of increasing ratio for higher AOD is evident for almost all schemes. The few outliers correspond to cases which were falsely assumed as clear skies. Due to the large scattering it is not feasible to derive firm quantitative estimates for the effect of aerosols. However, Fig. 5 suggests that this effect is likely of the order of 3–5% per 0.1 unit of AOD for all schemes except GFDL. The later seems to be less dependent on AOD, but at the same time very noisy. The pattern of the AOD

Table 5
Maximum availability of common hourly data for the AERONET (AOD) and HNSE (GHI) stations used in the analysis.

	Number of data per month				Annual total
	Jan.	Apr.	Jul.	Oct.	
Athens	4	43	110	–	158
Finokalia	4	48	15	–	67
Thessaloniki	3	–	95	36	134
Xanthi	–	20	–	–	20

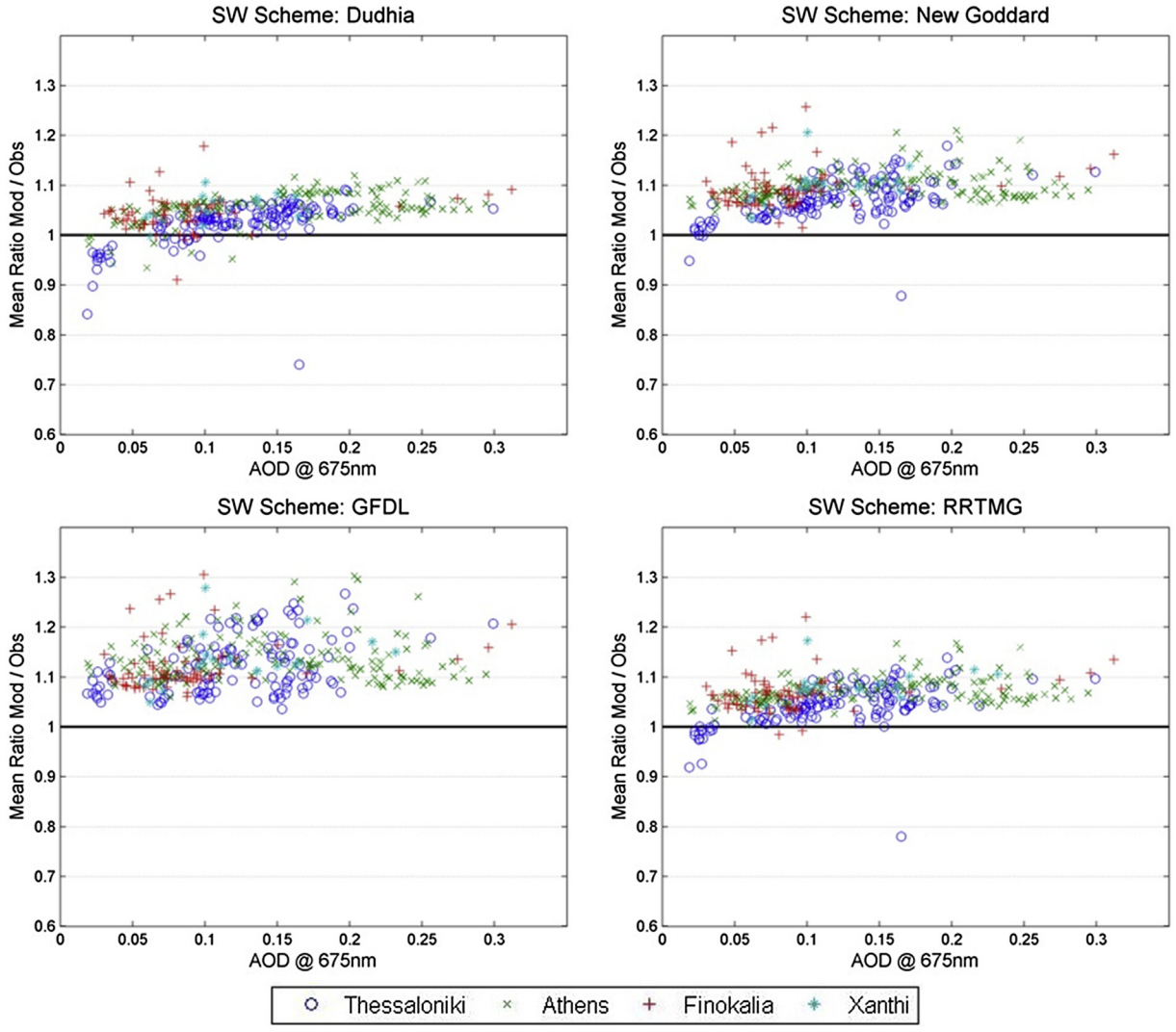

Fig. 5. Ratio of model-derived to measured GHI as a function of AOD at 675 nm derived from collocated Cimel sun-photometers at four HNSE stations. Each panel corresponds to a different SW scheme used in the model.

dependence is very similar for all four stations examined, which increases the robustness of the results.

The same analysis was repeated for AOD at other wavelengths (e.g., 500, 870 and 1020 nm), without showing any particular difference, neither in the pattern, nor in the absolute values, but 675 nm was chosen because AOD measurements at this wavelength was available at all 4 stations. The dependence of the predicted GHI on aerosols constitutes an important drawback for the Dudhia, RRTMG and New Goddard schemes. In many mid- and low-latitude locations, where solar insolation is strong, aerosols are important attenuators of solar radiation, particularly in the summer; therefore the present study can be a first valuable step for further investigation of model GHI predictions in Greece and could be used for post-processing methods accounting for AOD-dependent factors and cloud attenuation predictability.

4. Conclusions

In this study, solar irradiance data (GHI) for 2013 from a network of pyranometers deployed in Greece (HNSE) have been used to evaluate predictions of the WRF model using four SW radiation schemes: Dudhia, RRTMG, new Goddard and GFDL. The comparisons are certainly affected by spatial differences between the model outputs that are representative of a large area (10×10 km^2) while the pyranometer data refer to a single point. Particularly under cloudy conditions these differences become much more important.

It has been found that all schemes show a dependence on solar zenith angle, resulting in increasing overestimation of predicted GHI with increasing SZA. For clear sky conditions, this dependence is small for the Dudhia scheme and increases to up to 30% for RRTMG and New Goddard and up to 40% for GFDL. Moreover, all schemes generally overestimate the GHI, even at small SZAs. These two factors affect significantly the comparisons of the model predictions with the measurements, particularly when comparing hourly data. For clear-sky conditions the mean relative differences of hourly data for SZA smaller than 70° are between −2% and 7% for all schemes except GFDL (~12%), with relative standard deviations of about 15%. This level of agreement is worse to that reported by Ruiz-Arias et al. [45] for 5 sites in the US, who found relative differences of between −2 and 4% and about 4 times smaller RMSE. However in their study they compared only 5 clear days per station, while here we have used a range of days covering a whole year.

Under all-sky conditions the comparison is much worse, as the model derived GHI is largely overestimated. For the Dudhia scheme the mean relative difference is ~42% and for the other three schemes range between 56 and 73%. The variability of the results is

enormous with relative standard deviations exceeding 200% and for GFDL 300%. This behavior is generally consistent for all 12 stations and suggests that, for hourly data, none of the schemes can represent successfully the cloud effects on GHI. We were not able to detect a spatial behavior of the model performance according to the cloud regimes as defined by Zagouras et al. [59].

All SW radiation schemes are found to result to better GHI predictions during the warm period (April and July), likely due to the reduced presence of clouds. Particularly October, is associated with the greatest GHI overestimations when all sky conditions are considered.

In the comparisons of daily data, the time integration suppresses the variability of the hourly data, and the differences between model and measurements become smaller especially for all sky conditions. Subsequently the relative standard deviations are reduced to about half of those for hourly data. The Dudhia scheme performs best (mean relative difference 2.3 ± 7.7% (1σ) for clear skies and ~24 ± 80% for all skies). Although the results for the daily irradiation are generally consistent for all stations of HNSE, however, deviations of up to ~10% (15% for GFDL) can be detected among stations for clear skies. For all-sky conditions these deviations are twice as large.

Clouds and aerosols are the main factors influencing the model predictions of GHI and in turn their comparison with measurements. Clouds are produced stochastically in the model, so their exact position and properties deviate significantly from reality. This is more important for scattered cloud conditions because the relative position of the clouds and the measurement point determines whether the most abundant direct solar radiation is blocked or transmitted. Spatial or temporal averaging of predicted GHI can smooth the effects of clouds and improve the statistics of the comparisons with measurements, without improving, however, the accuracy of the predictions for the actual conditions. From the comparisons presented in this study, it appears that in most cases the model overestimates the cloud effects. This means that for each station, and possibly season, statistical corrections could be derived for adjusting the model predictions under all-sky conditions which are expected to improve in a statistical sense the model predictions.

Aerosols, can affect significantly the GHI mainly under clear-sky conditions, when the stronger effects of clouds are eliminated. By correlating the model-to-measurement GHI ratios with aerosol optical depth data at four stations, it appears that aerosols have a significant effect leading to an overestimation of the model predictions of the order of 3–5% per 0.1 unit of AOD at 675 nm. For the observed range of AOD at the 4 sites (between 0 and 0.3 units) the overestimation of GHI by the model can be between 9 and 15%. An improved representation of the effects of aerosols should be expected if short term forecasts of aerosols, that are already available, are coupled to the radiation schemes of the NWP models and taken into account either implicitly [46] or explicitly by post processing procedures. However, the predictability of the aerosol optical properties that determine to a great extent the attenuation of solar radiation is not yet mature enough for incorporation in to the radiation schemes. The results of the comparisons between model predicted GHI under clear skies and measurements can be used to derive site- and season-depended corrections of the model predictions for aerosol effects. However, this can be applied only for the specific locations and not generally for the entire model domain. An improvement should be expected from the incorporation of satellite-derived climatology of aerosol optical properties in the radiation schemes.

The results presented in this work suggest that the four shortwave radiation schemes that were used in WRF to predict GHI can lead to significant overestimations under all sky conditions. However, under clear skies and low to medium aerosol loads the performance of the four schemes is substantially improved. This study aimed mainly to detect weaknesses of the application of the WRF model as a first step towards improvement of GHI predictions over Greece. The findings can be used as a guide for applications of WRF for solar energy applications in regions with medium to high aerosol loads, while they could also be used by model developers for improving the relevant algorithms of the radiation schemes.

Acknowledgments

The authors acknowledge funding by the Greek State Scholarships Foundation (Grant No: SR 22088/13) and Siemens AG under the "IKY-Siemens Post-doctoral Scholarship Programme 2013–2014".

The authors would also like to thank PIs of the AERONET stations used in this study, namely Prof. Spyros Rapsomanikis (Xanthi station), Dr. Vassilis Amiridis (Athens station) and Dr. Andrew Clive Banks (FORTH Crete station).

Dr. Jimy Dudhia is also acknowledged for his valuable remarks during the realization of this study.

The authors acknowledge the General Secretariat for Research and Technology, Greek Ministry of Education, Lifelong Learning and Religious Affairs for funding the project Hellenic Network of Solar Energy (www.helionet.gr, 09SYN-32-778).

MeteoSwiss is acknowledged for providing the instruments for the establishment of the HNSE ground-based network.

A. Kazantzidis acknowledges the European Commission for funding the project DNICast (www.dnicast-project.net), grant agreement: 608623.

References

[2] A. Bais, A. Kazantzidis, C. Zerefos, D. Melas, E. Kosmidis, S. Kazadzis, E. Nikitidou, T.M. Giannaros, M.M. Zempila, K. Fragkos, V. Salamalikis, Hellenic Network for Solar Energy, Advances in Meteorology, Climatology and Atmospheric Physics, Springer Atmospheric Sciences, Springer Berlin, Heidelberg, 2013, http://dx.doi.org/10.1007/978-3-642-29172-2_55.

[3] J. Boland, Spatial-temporal forecasting of solar radiation, Renew. Energy. ISSN: 0960-1481 75 (2015) 607–616. http://dx.doi.org/10.1016/j.renene.2014.10.035.

[7] D. Burnett, E. Barbour, G.P. Harrison, The UK solar energy resource and the impact of climate change, Renew. Energy. ISSN: 0960-1481 71 (2014) 333–343. http://dx.doi.org/10.1016/j.renene.2014.05.034.

[8] F. Chen, J. Dudhia, Coupling an advanced land surface-hydrology model with the Penn State-NCAR MM5 modeling system, Part I: model implementation and sensitivity, Mon. Weather Rev. 129 (2001) 569–585.

[9] M.-D. Chou, M.J. Suarez, A Solar Radiation Parameterization (CLIRAD-SW) Developed at Goddard Climate and Radiation Branch for Atmospheric Studies, Goddard Space Flight Center, Greenbelt, 1999. NASA Tech. Memo., NASA/TM-1999–104606(15).

[10] A.E. Curtright, J. Apt, The character of power output from utilityscale photovoltaic systems, Prog. Photovolt. Res. Appl. 16 (3) (2008) 241–247.

[11] J. Dudhia, Numerical study of convection observed during the winter monsoon experiment using a mesoscale two-dimensional model, J. Atmos. Sci. 46 (1989) 3077–3107, http://dx.doi.org/10.1175/1520-0469(1989)046.

[12] A. Economou, Photovoltaic systems in school units of Greece and their consequences, Renew. Sustain. Energy Rev. 15 (2011) 881–885.

[13] J.G. Fantidis, D.V. Bandekas, C. Potolias, N. Vordos, Cost of PV electricity – Case study of Greece, Sol. Energy 91 (2013) 120–130.

[14] S.B. Fels, M.D. Schwarzkopf, An efficient, accurate algorithm for calculating CO2 15μ band cooling rates, J. Geophys. Res. 86 (1981) 1205–1232.

[15] A. Fernández-García, E. Zarza, L. Valenzuela, M. Perez, Parabolic-trough solar collectors and their applications, Renew. Sustain. Energy Rev. 14 (2010) 1695–1721.

[16] E. Gerasopoulos, M.O. Andreae, C.S. Zerefos, T.W. Andreae, D. Balis, P. Formenti, P. Merlet, V. Amiridis, C. Papastefanou, Climatological aspects of aerosol optical properties in Northern Greece, Atmos. Chem. Phys. 3 (2003) 2025–2041, http://dx.doi.org/10.5194/acp-3-2025-2003.

[17] B. Greening, A. Azapagic, Domestic solar thermal water heating: A sustainable option for the UK? Renew. Energy. ISSN: 0960-1481 63 (2014) 23–36. http://dx.doi.org/10.1016/j.renene.2013.07.048.

[18] G. Grell, J. Dudhia, D. Stauffer, A Description of the Fifth-generation Penn State/NCAR Mesoscale Model (MM5), 1998. NCAR Tech. Note, NCAR/TN-398+STR, USA.

[19] G.A. Grell, D. Deveniy, A generalized approach to parameterizing convection

combining ensemble and data assimilation techniques, Geophys. Res. Lett. 29 (2002) L15311.
[20] C.A. Gueymard, Turbidity determination from broadband irradiance measurements: a detailed multi-coefficient approach, J. Appl. Meteorol. 37 (4) (1998) 414–435.
[21] E. Hart, E. Stoutenburg, M. Jacobson, The potential of intermittent renewables to meet electric power demand: current methods and emerging analytical techniques, Proc. IEEE 100 (2) (2012) 322–334.
[22] D. Heinemann, E. Lorenz, M. Girodo, Forecasting of solar radiation, in: E.D. Dunlop, L. Wald, M. Šúri, E.D. Dunlop (Eds.), Solar Energy Resource Management for Electricity Generation from Local Level to Global Scale, Nova Science Publishers, New York, 2006.
[23] Hellenic Ministry of Environment, Energy and Climate Change. National Renewable Energy Action Plan in the Scope of Directive 2009/28/EC, 2010.
[25] M.J. Iacono, J.S. Delamere, E.J. Mlawer, M.W. Shephard, S.A. Clough, W.D. Collins, Radiative forcing by long-lived greenhouse gases: calculations with the AER radiative transfer models, J. Geophys. Res. 133 (2008) D13103.
[26] IEA, Electricity Information 2012, Published by the International Energy Agency, 2012, 883 pp.
[27] IEA, World Energy Outlook 2014, Executive Summary, Published by the International Energy Agency, 2014.
[28] R.H. Inman, H.T.C. Pedro, C.F.M. Coimbra, Solar forecasting methods for renewable energy integration, Prog. Energy Combust. Sci. 39 (6) (2013) 535–576.
[29] Z.I. Janjic, The step-mountain eta coordinate model: further developments of the convection, viscous, sublayer and turbulence closure schemes, Mon. Weather Rev. 122 (1994) 927–945.
[30] S. Kiliccote, P. Price, M.A. Piette, G. Bell, S. Pierson, E. Koch, J. Carnam, H.T.C. Pedro, J. Hernandez, A. Chiu, Field Testing of Automated Demand Response for Integration of Renewable Resources in California's Ancillary Services Market for Regulation Products, 2012. Tech. rep.
[31] V. Lara-Fanego, J.A. Ruiz-Arias, D. Pozo-Vázquez, et al., Evaluation of the WRF model solar irradiance forecasts in Andalusia (southern Spain), Sol. Energy 86 (2012) 2200–2217.
[32] M. Lave, J. Stein, A. Ellis, C. Hansen, E. Nakashima, Y. Miyamoto, Ota City: Characterizing Output Variability from 553 Homes with Residential PV Systems on a Distribution Feeder, Tech. rep, Sandia National Laboratories, Albuquerque, NM, 2011.
[33] E. Lorenz, J. Hurka, D. Heinemann, H.G. Beyer, Irradiance forecasting for the power prediction of grid-connected photovoltaic systems, IEEE J. Sel. Top. Appl. Earth Obs. Remote Sens. 2 (1) (2009b).
[34] E. Lorenz, J. Remund, S.C. Müller, et al., Benchmarking of different approaches to forecast solar irradiance, in: 24th European Photovoltaic Solar Energy Conference, Hamburg, Germany, 2009, pp. 21–25. September 2009.
[35] J. Marcos, L. Marroyo, E. Lorenzo, M. Garca, Smoothing of PV power fluctuations by geographical dispersion, Prog. Photovolt. Res. Appl. 20 (2) (2012) 226–237.
[36] A.P. Matzarakis, V.D. Katsoulis, Sunshine duration hours over the Greek region, Theor. Appl. Climatol. 83 (2006) 107–120, http://dx.doi.org/10.1007/s00704-005-0158-8.
[37] B. Mayer, A. Kylling, Technical note: the libRadtran software package for radiative transfer calculations - Description and examples of use, Atmos. Chem. Phys. 5 (2005) 1855–1877, http://dx.doi.org/10.5194/acp-5-1855-2005.
[38] A. Mellit, A.M. Pavan, A 24-h forecast of solar irradiance using artificial neural network: application for performance prediction of a grid-connected PV plant at Trieste, Italy, Sol. Energy 84 (5) (2010) 807–821.
[39] D. Neves, C.A. Silva, Modeling the impact of integrating solar thermal systems and heat pumps for domestic hot water in electric systems – The case study of Corvo Island, Renew. Energy. ISSN: 0960-1481 72 (2014) 113–124. http://dx.doi.org/10.1016/j.renene.2014.06.046.
[40] C.D. Papadimas, N. Hatzianastassiou, N. Mihalopoulos, X. Querol, I. Vardavas, Aerosol Optical Depth variability in the Mediterranean basin based on MODIS and AERONET data, J. Geophys. Res. 113 (2008) D11205, http://dx.doi.org/10.1029/2007JD009189.
[41] R. Perez, S. Kivalov, J. Schlemmer, et al., Validation of short and medium term operational solar radiation forecasts in the US, in: Proceedings of the ASES Annual Conference, Buffalo, New York, 2009.
[42] R. Perez, E. Lorenz, S. Pelland, et al., Comparison of numerical weather prediction solar irradiance forecasts in the US, Canada and Europe, Sol. Energy 94 (2013) 305–326.
[43] R. Remund, R. Perez, E. Lorenz, Comparison of solar radiation forecasts for the USA, in: Proceedings of the 23rd European Photovoltaic Solar Energy Conference, 2008, Valencia, Spain, 2008, pp. 1.9–4.9.
[44] J.A. Ruiz-Arias, H. Alsamamra, J. Tovar-Pescador, D. Pozo-Vázquez, Proposal of a regressive model for the hourly diffuse solar radiation under all sky conditions, Energy Convers. Manag. 51 (5) (2010) 881–893.
[45] J.A. Ruiz-Arias, J. Dudhia, F.J. Santos-Alamillos, D. Pozo-Vázquez, Surface clear-sky shortwave radiative closure intercomparisons in the Weather Research and Forecasting model, J. Geophys. Res. Atmos. 118 (2013) 1–13, http://dx.doi.org/10.1002/jgrd.50778.
[46] J.A. Ruiz-Arias, C.A. Gueymard, F.J. Santos-Alamillos, D. Pozo-Vázquez, Do spaceborne aerosol observations limit the accuracy of modeled surface solar irradiance? Geophys. Res. Lett. 42 (2015) 605–612, http://dx.doi.org/10.1002/2014GL062309.
[47] J.A. Ruiz-Arias, D. Pozo-Vázquez, N. Sánchez-Sánchez, et al., Evaluation of two MM5-PBL parameterizations for solar radiation and temperature estimation in the South-Eastern area of the Iberian Peninsula, Il Nuovo Cim. 31 (5–6) (2008) 825–842.
[48] V. Salas, E. Olias, Overview of the photovoltaic technology status and perspective in Spain, Renew. Sustain. Energy Rev. 13 (5) (2009) 1049–1057.
[49] J.J. Sarralde, D.J. Quinn, D. Wiesmann, K. Steemers, Solar energy and urban morphology: scenarios for increasing the renewable energy potential of neighbourhoods in London, Renew. Energy. ISSN: 0960-1481 73 (2015) 10–17. http://dx.doi.org/10.1016/j.renene.2014.06.028.
[50] W.C. Skamarock, J.B. Klemp, J. Dudhia, et al., A Description of the Advanced Research WRF Version 3. NCAR/TN-475+STR, Mesoscale and Microscale Meteorology Division, National Centre for Atmospheric Research, Boulder, USA, 2008.
[51] F. Sobhnamayan, F. Sarhaddi, M.A. Alavi, S. Farahat, J. Yazdanpanahi, Optimization of a solar photovoltaic thermal (PV/T) water collector based on exergy concept, Renew. Energy. ISSN: 0960-1481 68 (2014) 356–365. http://dx.doi.org/10.1016/j.renene.2014.01.048.
[52] M. Šúri, T.A. Huld, E.D. Dunlop, H.A. Ossenbrink, Potential of solar electricity generation in the European Union member states and candidate countries, Sol. Energy. ISSN: 0038-092X 81 (10) (October 2007) 1295–1305. http://dx.doi.org/10.1016/j.solener.2006.12.007.
[53] P. Szuromi, B. Jasny, D. Clery, et al., Energy for the long haul, Science 315 (5813) (2007) 781.
[54] G. Thompson, P.R. Field, R.M. Rasmussen, W.D. Hall, Explicit forecasts of winter precipitation using an improved bulk microphysics scheme, Part II: implementation of a new snow parameterization, Mon. Weather Rev. 136 (2008) 5095–5115.
[55] G. Thompson, R.M. Rasmussen, K. Manning, Explicit forecasts of winter precipitation using an improved bulk microphysics scheme, Part I: description and sensitivity analysis, Mon. Weather Rev. 132 (2004) 519–542.
[56] E. Wiemken, H.G. Beyer, W. Heydenreich, K. Kiefer, Power characteristics of PV ensembles: experiences from the combined power production of 100 grid connected PV systems distributed over the area of Germany, Sol. Energy 70 (6) (2001) 513–518.
[58] M. Wittmann, H. Breitkreuz, M. Schroedter-Homscheidt, M. Eck, Case-studies on the use of solar irradiance forecast for optimized operation strategies of solar thermal power plants, IEEE J. Sel. Top. Appl. Earth Obs. Remote Sens. 1 (1) (2008) 18–27.
[59] A.A. Zagouras, A. Kazantzidis, E. Nikitidou, A.A. Argiriou, Determination of measuring sites of solar irradiance, based on cluster analysis of satellite-derived cloud estimations, Sol. Energy 97 (2013) 1–11.
[60] A. Zagouras, Hugo T.C. Pedro, Carlos F.M. Coimbra, Clustering the solar resource for grid management in island mode, Sol. Energy 110 (2014) 507–518.
[61] R.J. Zamora, E.G. Dutton, M. Trainer, et al., The accuracy of solar irradiance calculations used in mesoscale numerical weather prediction, Mon. Weather Rev. 133 (2005) 783–792.
[62] R.J. Zamora, S. Solomon, E.G. Dutton, Comparing MM5 radiative fluxes with observations gathered during the 1995 and 1999 Nashville southern oxidant studies, J. Geophys. Res. 108 (D2) (2003) 4050.